CALICE Analysis Note CAN-049
May, 2014

Analogue, Digital and Semi-Digital Energy Reconstruction in the CALICE AHCAL

The CALICE Collaboration

Abstract

In this note, different energy reconstruction methods for the Analogue Hadronic Calorimeter (AHCAL) are compared. These methods were developed for the analogue, digital and semi-digital CALICE Hadronic Calorimeter physics prototypes and were used in analyses of data taken at various test beams.
The analogue data can also provide digital information, thus the advantages and disadvantages of different energy reconstruction procedures can be studied in the same data sample. In this work this comparison is done by applying these procedures to AHCAL pion test beam data collected with the 1 m^3 physics prototype in 2007 at CERN. The results are compared to a GEANT4 based simulation.

[1]Corresponding authors:
Coralie Neubüser; coralie.neubueser@desy.de
Katja Krüger; katja.krueger@desy.de

Contents

1 Introduction

For a future linear electron-positron collider like ILC or CLIC, the desired jet energy resolution of $3 - 4\,\%$ for a wide range of jet energies can be achieved by using Particle Flow Algorithms for the jet reconstruction. Within the CALICE collaboration, several concepts for a hadron calorimeter (HCAL) optimised for Particle Flow are studied and have been tested with large, $\sim 1\,\mathrm{m}^3$ prototypes: the so-called analogue, digital and semi-digital HCAL concepts. The concepts differ in active material for the shower detection, granularity, readout technology and reconstruction method. This makes it difficult to disentangle the influence of each of these components to the energy resolution of jets as well as of individual particles. Since the analogue HCAL prototype has a larger cell size than the other two concepts, and the digital and semi-digital HCAL prototypes do not provide analogue hit size information, it is impossible to study all different aspects in test beam data. For the data taken with the analogue HCAL prototype, a direct comparison of the reconstruction methods is possible, albeit with a cell size not optimal for the digital and semi-digital methods. The effect of the other differences can only be studied directly in simulation, where every aspect can be changed separately. For reliable results from the simulation it is important to validate the simulation of hadronic showers in the detector prototypes by comparing them to the measured test beam data, especially for the quantities that are relevant for the energy reconstruction.

In this note, pion test beam data taken with the prototype of the analogue HCAL are used to apply also the readout concept and reconstruction procedures developed for the digital and semi-digital HCAL. Thus, the three reconstruction methods can be compared based on the same data set, with identical active material and identical granularity. The results are compared with a simulation based on the GEANT4 software package.

2 Energy reconstruction procedures

For the three different CALICE Hadronic Calorimeters, which use different active material and readout, three different energy reconstruction procedures are developed, which will be discussed in detail in the following.

2.1 Analogue

The Analogue HCAL is a scintillator tile calorimeter with individual Silicon Photomultiplier (SiPM) read-out. Within the scintillating plastic the charged particles excite the scintillator which emits photons. These photons are captured by a wavelength-shifting fiber that transports the light to the SiPM. During calibration the measured ADC counts of the SiPM are converted to the response of a muon or minimum-ionizing particle (MIP), see [1].

Within several test beam campaigns a 1 m^3 physics prototype was tested and its single particle resolution was validated [2]. This prototype consists of up to 38 HCAL layers with the first 30 layers of three different tile sizes; 12x12, 6x6 and 3x3 cm^2 and the last 8 layers of only 6x6 and 12x12 cm^2 tiles.

The visible signal for the energy reconstruct is calculated in units of MIP as a sum of cell signals above 0.5 MIP which are called hits. The 0.5 MIP threshold is used to reject noise. The MIP scale is converted to GeV scale using electromagnetic calibration factors ω which was determined from the dedicated positron runs in [3]. The Sc-Fe AHCAL is a non-compensating calorimeter, as its response to electrons is by factor of $e/\pi = 1.19$ higher than to pions of the same energy [2]. Then the reconstructed energy in the AHCAL for each pion event is calculated as follows:

$$E_{rec,analogue} = \frac{e}{\pi} \cdot \omega \cdot E_{sum} \tag{1}$$

2.2 Digital

The Digital HCAL is a sandwich calorimeter with Resistive Plate Chambers (RPCs) as active material. An RPC consists of glass and a 1.15 mm gas gap, read out by pad electrodes of 1x1 cm^2 size placed on the back of the plates. The incoming particles traverse the gas, ionize it and the induced charges get amplified by the applied high voltage. The charge multiplication is quenched by the high resistivity of the glass.

The measurement observable is the total number of hits in the HCAL. There is no information about the signal size. A calibration is done by equalizing the response to obtain an average multiplicity and efficiency for muons (MIP) in every layer. More sophisticated calibration procedures are under investigation, see [4].

Within the energy reconstruction a correction of the non-linearity is applied. The non-linearity arises from multiple particles traversing the same pad, limited granularity and binary information. Several approaches have been developed to correct for this non-linearity. Here, a simple approach is followed by fitting the mean response versus beam energy with a power law as $\langle N_{hits} \rangle = a \cdot (E_{beam})^b$ and taking the extracted parameters a and b for the reconstruction on an event-by-event basis as follows:

$$E_{rec,digital} = \sqrt[b]{\frac{N_{hits}}{a}} \tag{2}$$

2.3 Semi-digital

The principle of the semi-digital HCAL is similar to digital HCAL, but with a 2-bit read-out. A large SDHCAL prototype has been realised with RPCs. In addition several MICROMEGAS layers have been tested. The granularity of the read-out of these devices was also 1x1 cm^2. The difference between both is the active material, while the calorimeter principle is the same. The 2-bit read-out codes the information of 3 thresholds. This additional information compared to the DHCAL has the goal to identify multiple particles contributing to the signal of a pad. First results of test beams of the RPC SDHCAL physics prototype are shown in [5]. We will follow the same way of energy reconstruction here: Reconstructing the energy as a sum of the weighted number of hits for the 3 thresholds, $E_{rec,semi-digital}$ can be written as a function of N_1, the number of hits above the first and below the second; N_2, the number of hits above the second below the third; and N_3, the number of hits above the third threshold:

$$E_{rec,semi-digital} = \alpha N_1 + \beta N_2 + \gamma N_3, \tag{3}$$

with the weights α,β and γ. Hadronic showers change their structure and evolution with energy, which is taken into account by parameterizing α,β and γ as quadratic polynomials of the total number of hits $N_{hits} = N_1 + N_2 + N_3$. To find the best parameterization of these so called calibration coefficients, a χ^2-like function of the form

$$\chi^2 = \sum_{i=1}^{N} \frac{\left(E^i_{beam} - E^i_{rec,semi-digital}\right)^2}{E^i_{beam}}, \tag{4}$$

is minimised, where i runs over all events.

3 Data and Simulations

For this analysis the AHCAL test beam data from 2007 with steel absorber is chosen. The reason for this choice was the good understanding of the data, validated by several published CALICE analyses [1, 2, 6, 7].
The 2007 CERN test beam setup consisted of 30 layers of CALICE silicon-tungsten ECAL, 38 layers of the scintillator-steel analogue HCAL and 16 layers of the scintillator-steel tail catcher and muon tracker (TCMT). The absorber thickness for the ECAL varied between 1.4, 2.8 and 4.2 mm and radiation lengths 0.4, 0.8 and 1.2 X_0, the one of the HCAL was ~ 2 cm. A detailed description of the test beam setup can be found in [7].

3.1 Run & event selection

The data samples are selected from π^- data in the range of 10 to 80 GeV. The run list and event selection follows the published software compensation analysis [2] and is summarised in table 1. The events of runs with the same beam energy are merged and undergo the same requirements for the π^- event selection.
The data sample is reconstructed with the newest calice_soft version v04-08.
After the pre-selection information of π^- events using the Cherenkov counter and the reduction of noise by applying a threshold of 0.5 MIP on every cell, we reject

- muon and punch-through pion events by requiring more than 150 MIP deposited in the AHCAL.
- multi-particle events by requiring less than 80 MIP and 13 hits in the first 5 layers of the AHCAL.
- empty events by requiring more than 25 hits in the ECAL and 50 hits in the AHCAL.

For further sample purity, we select π^- events to

- start showering in the first 5 HCAL layers by the ShowerStartClusterProcessor, details can be found in [8].
- be consistent with a MIP-like particle by requiring less than 50 hits in the ECAL.

The selected pion showers develop predominantly in the AHCAL while keeping the energy leakage into the TCMT as small as possible. Examples of the distributions of E_{sum} and N_{hits} after the pre-selection and after the full analysis selection are shown for two beam energies in Figure 1.

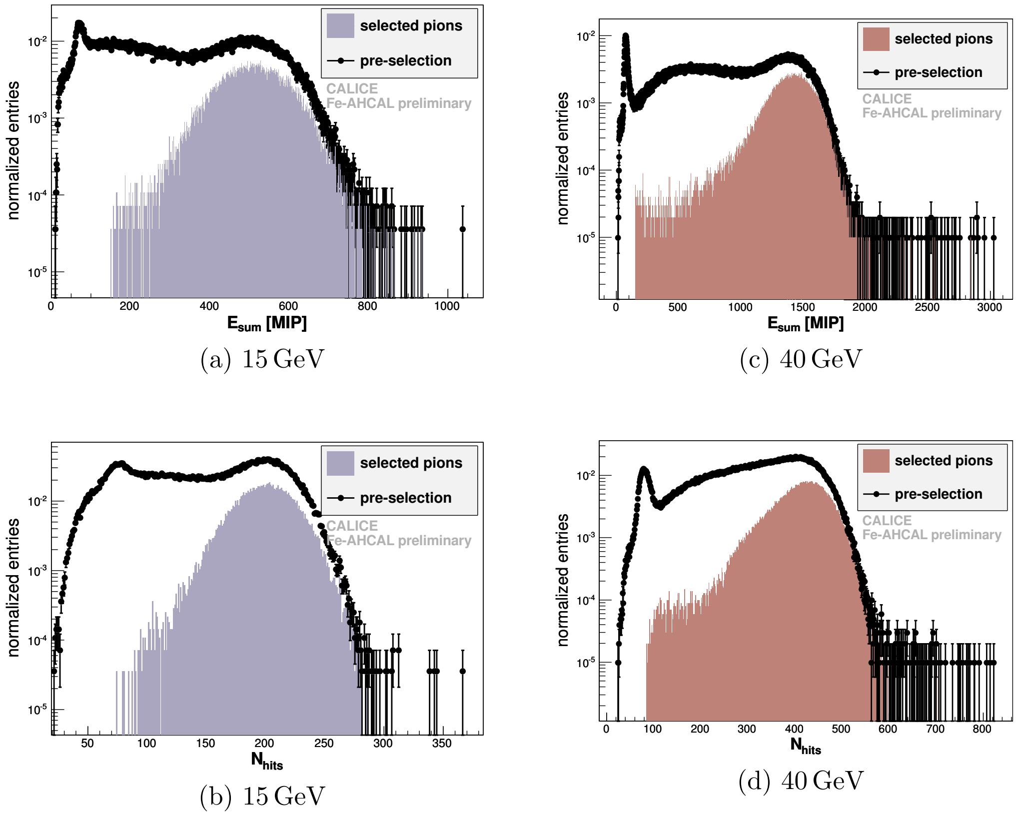

(a) 15 GeV (b) 15 GeV (c) 40 GeV (d) 40 GeV

Figure 1: Distributions of the visible energy E_{sum} and number of hits N_{hits} in the AHCAL for 15 GeV in 1a, 1b and 40 GeV in 1c, 1d for the events preselected using Cherenkov counter (black points) and for the selected events (filled histograms).

3.2 Monte Carlo model

The test beam runs are simulated using the software packages GEANT4 version 9.6 patch 1, Mokka v08_02 and ilcSoft v01_17_05, followed by digitisation using calice_soft v04-08 with the conversion coefficients 846 keV/MIP and 15 % optical crosstalk between the AHCAL tiles. As the physics list FTFP_BERT from GEANT4 9.6 shows best performance for hadrons, it was chosen for comparisons in this analysis. All

Table 1: List of data runs used in the analysis and sample statistics. The size of each simulated sample is 100,000 events per run.

run number	beam energy [GeV]	pre-selection data	selected pions in data	in %	selected pions in MC	in %
330332, 330643, 330777, 330850	10	587,793	111,133	18.9	81,974	20.5
330328	15	140,441	28,024	20.0	21,063	21.1
330327	18	148,516	29,600	19.9	21,040	21.0
330649, 330771	20	379,270	73,942	19.5	41,718	20.9
330325, 330650	25	364,170	72,530	19.9	41,474	20.7
330551, 330960	35	404,309	70,438	17.4	40,868	20.4
330390, 330412, 330560	40	509,168	101,617	20.0	61,394	20.5
330550, 330559, 330961	45	520,600	102,898	19.8	61,181	20.4
330391, 330558	50	384,581	76,855	20.0	41,081	20.5
331556, 331568, 331655, 331664	60	787,208	153,464	19.5	81,565	20.4
330392, 330962, 331554, 331567, 331654	80	898,307	176,476	19.7	100,278	20.1

test beam runs listed in table 1 were simulated with 100,000 π^- events, the noise being added to the digitised samples from the corresponding runs. Afterwards, the simulated samples of the same energy were merged and the same selection procedure was applied as to the data samples. The resulting number of pion events and the percentage of selected events are given in table 1.

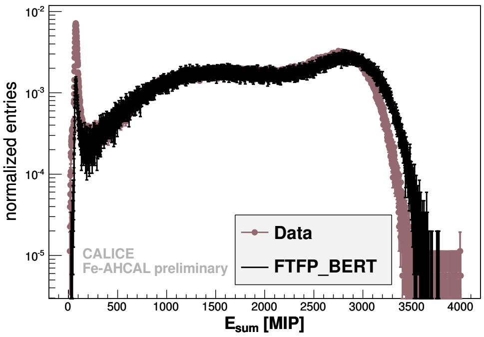

(a) pre-selection

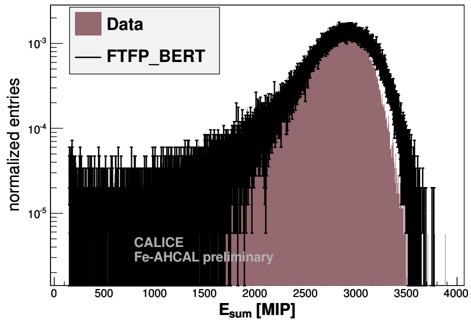

(c) final selection

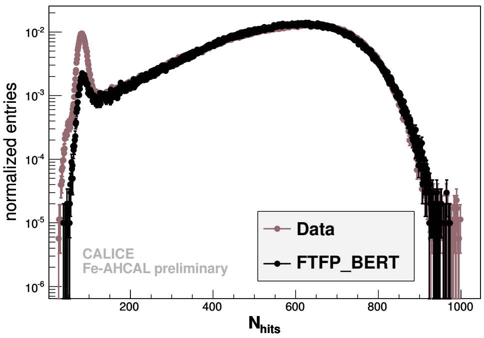

(b) pre-selection

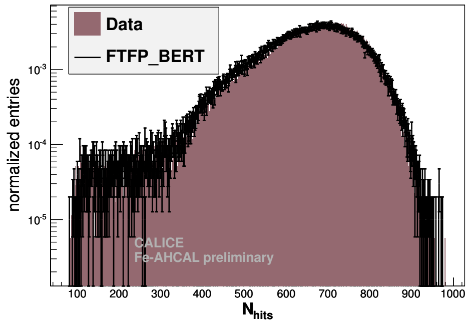

(d) final selection

Figure 2: Distributions of the visible energy E_{sum} and the number of hits N_{hits} for $E_{beam} = 80\,\mathrm{GeV}$ for the pre-selection and the final π^- selection. The simulated FTFP_BERT data is shown as black points while the data is given as colored and filled histograms.

Figures 2 and 3 show the distributions of the visible energy and the number of hits in the AHCAL for data and MC for 10 and 80 GeV. For all other energies the differences between data and MC are smaller. In all pre-selection plots for the energy sum distributions (see Figure 2a, 3a) and the corresponding number of hits (see Figure 2b,3b) a higher peak at 100 MIP, 40 hits respectively is seen in data than the FTFP_BERT sample. This is due to the muon contamination in data, while in MC this peak arises only from punch-through pions. A second effect is in general an slight overestimation in the FTFP_BERT samples for the number of hits. This can be seen in Figure 3d, where the FTFP_BERT distribution ahows a slightly higher number of hits, while the energy sum of the FTFP_BERT samples is consistent with data until 60 GeV. The largest difference is seen in Figure2c.

This trend to an overestimation of the AHCAL response by FTFP_BERT was already seen and studied in [9].

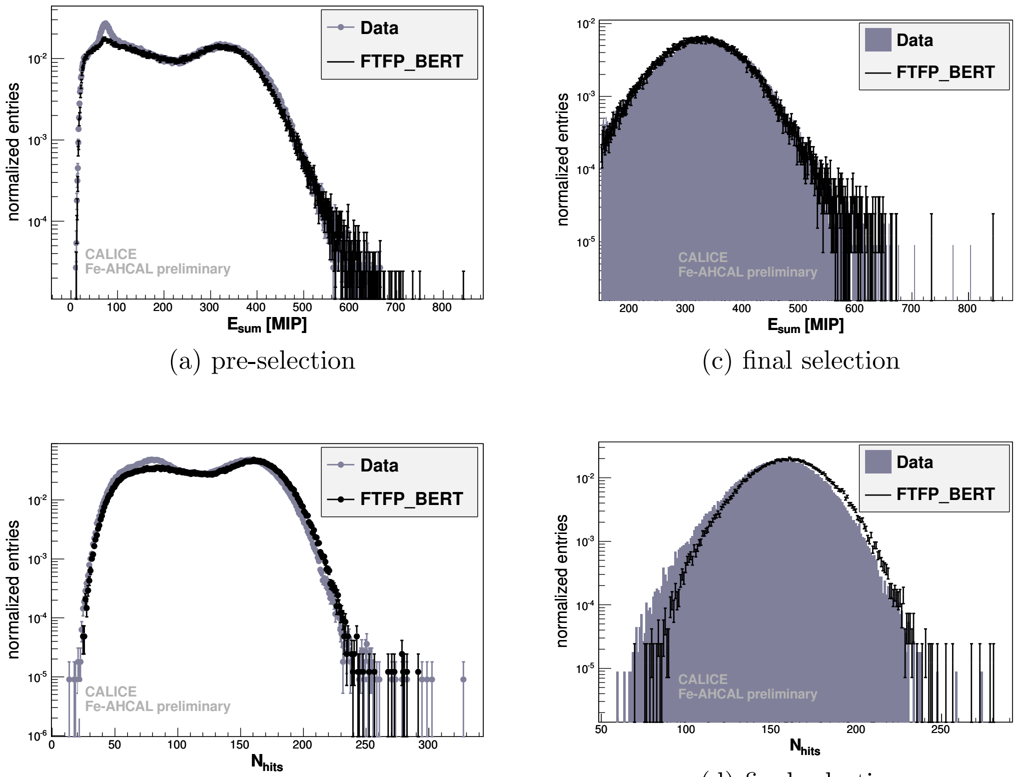

(a) pre-selection

(c) final selection

(b) pre-selection

(d) final selection

Figure 3: E_{sum} and N_{hits} for $E_{beam} = 10\,\mathrm{GeV}$ for the pre-selection and the final π^- selection. The simulated FTFP_BERT data is shown as black points while the data is given as colored and filled histograms.

3.3 Systematic uncertainties

The systematic uncertainties are estimated following [2] and [6], which both use the detailed analysis of the electromagnetic response [3]. Thus, the uncertainty of the beam energy ΔE_{beam} is taken into account with

$$\frac{\Delta E_{beam}}{E_{beam}} = \frac{12\%}{E_{beam}} \oplus 0.1\%. \tag{5}$$

The method how to determine these values was first described in [10].
The uncertainty on the reconstructed energy is dominated by the MIP to GeV conversion, which is estimated to be 0.9 %. The impact of the SiPM gain and saturation parameters are negligibly small [3].
In the following for the energies reconstructed from the energy sum the systematic uncertainty of the beam energy and the uncertainty from the MIP to GeV conversion are added in quadrature. For the energies reconstructed with the number of hits, the 0.9 % uncertainty from the MIP to GeV conversion is not taken into account.

4 Energy reconstruction and linearity

The goal of this analysis is a direct comparison of the three reconstruction methods, analogue, semi-digital and digital, applied to the same AHCAL data. This includes using the same methods to extract the mean energy and the resolution. Since the distributions of the energy reconstructed from the number of hits are expected to show a non-gaussian tail, the procedure to fit the distributions and to extract the mean and the width will be discussed and compared to previous AHCAL analyses.

4.1 Analogue

4.1.1 Comparison to previous analyses

Earlier studies of this test beam data used the entire setup for the energy reconstruction. The energy in the ECAL and the TCMT complemented the measurement of the HCAL, see [2]. The conversion factors from the visible to the deposited energy were estimated using simulations and data and were given for the three different sections of the ECAL with different sampling fractions and two sections of the TCMT. The values can be found in appendix A.

Here the goal is to study the details of the energy reconstruction in the HCAL. Therefore, to be independent on the reconstruction procedures of the other sub-detectors, the TCMT measurement is not used, while the ECAL measurement is only used for event selection. A fixed value of $0.3805 \pm 0.0003(stat.) \pm 0.0381(syst.)$ GeV is taken as contribution of the track in the ECAL to the total shower energy (see appendix A). The systematic error is estimated from the $\sim 10\,\%$ increasing deposited energy in the ECAL with increasing beam energy from 10 to 80 GeV. Thus the analogue reconstructed energy is given by

$$E_{rec,analogue} = 0.3805\,\mathrm{GeV} + \frac{e}{\pi}\left(\omega \cdot E_{sum}\right). \tag{6}$$

The $E_{rec,analogue}$ distributions are usually fitted with a gaussian function within $2\,\sigma$ standard deviation, compare [2]. The goal of this analysis is to study the differences between the reconstruction methods, thus for consistency the analogue response will be treated in the same way as the digital and semi-digital. This means that we use the Novosibirsk function

$$f(x) = A \cdot \exp\left(-\frac{1}{2} \cdot \left(\frac{\ln^2\left[1 + \Lambda \cdot \tau \cdot (x - \mu)\right]}{\tau}\right) + \tau^2\right) \tag{7}$$

with $\Lambda = \frac{\sin\left(\tau \cdot \sqrt{\ln 4}\right)}{\sigma \cdot \tau \cdot \sqrt{\ln 4}}$ to fit the $E_{rec,analogue}$ within $\mu \pm 3\,\sigma$ of a primarily Gaussian fit of the distributions. The fit every time provides a χ^2/ndf better than 3, usually better than 2. In order to extract the mean and the width of this fit function, a histogram is filled with random values generated according to this function with the extracted fit parameters σ,μ and τ. The range of this histogram is chosen to be from 0 to $\mu + 3\,\sigma$ of the fit function. The mean and RMS of the histogram are used as response and resolution for the studied energy. This procedure ensures that the extracted response and resolution are rather insensitive to single outliers, which could be caused e.g. by a remaining muon contamination of the pion sample, but it fully takes into account the possible asymmetry of the distribution.

In order to compare this procedure to the results of Gaussian fits in a $\pm 2\,\sigma$ range as used in previous AHCAL analyses, the distributions are also fitted with Gaussians. The $E_{rec,analogue}$ distributions are shown in Figure 4. Here it is seen that the $E_{rec,analogue}$ distributions show asymmetries for high energies, above 30 GeV, due to longitudinal energy leakage. In the previous analyses, this effect is not present since they take into account the energy deposited in the TCMT. Therefore, for the comparison with earlier results, we fitted a Gaussian in the range -1 and +2 standard deviations. The response and the deviation from linearity of the two procedures are compared in Figure 5. Both procedures show agreement with a linear behaviour within $\pm 2\,\%$. As expected from the tails to the left, the values extracted with the Novosibirsk are slightly lower than the Gaussian values, with the effect increasing with increasing beam energy up to $\sim 3\,\%$ at 80 GeV.

The resulting energy resolutions are shown in Fig. 6. They are also compared with the parametrised resolution determined in a previous analysis [2] with a stochastic term $a = 57.6 \pm 0.4\,\%$, constant term $b = 1.6 \pm 0.2\,\%$ and the noise term of $c = 0.18$ GeV:

$$\frac{\sigma_{rec}}{\langle E_{rec} \rangle} = \frac{a}{\sqrt{E_{beam}[GeV]}} \oplus b \oplus \frac{c}{E_{beam}[GeV]} \tag{8}$$

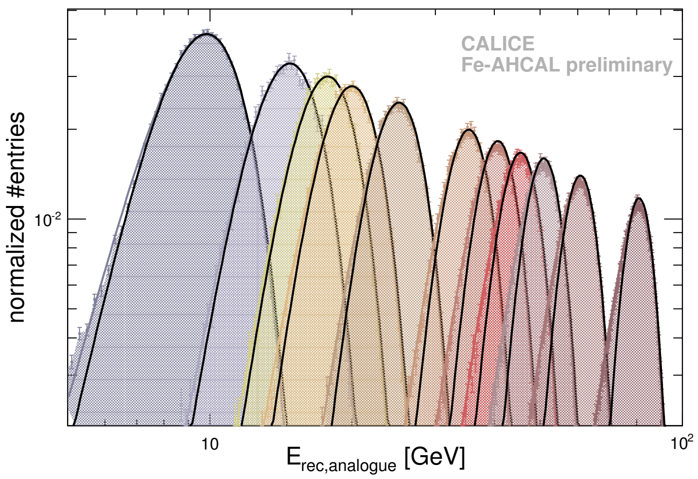

Figure 4: **Analogue reconstructed energy distributions** for pions with initial energies 10-80 GeV. The black curves show the Gaussian fit between -1 and $+2\,\sigma$.

The energy resolution determined with the Gaussian fits is slightly worse by about $0.5 - 1\,\%$ in absolute values than the resolution in the previous analysis, probably because of the simplified treatment of the ECAL contribution and the removal of the TCMT measurement from the energy reconstruction procedure. As expected, including the tail of the distributions due to energy leakage by taking the mean and RMS from the Novosibirsk function increases $\sigma_{rec}/\langle E_{rec} \rangle$. This effect is very small at 10 GeV and increases up to absolute $\sim 3\,\%$ at 80 GeV. It should be noted here

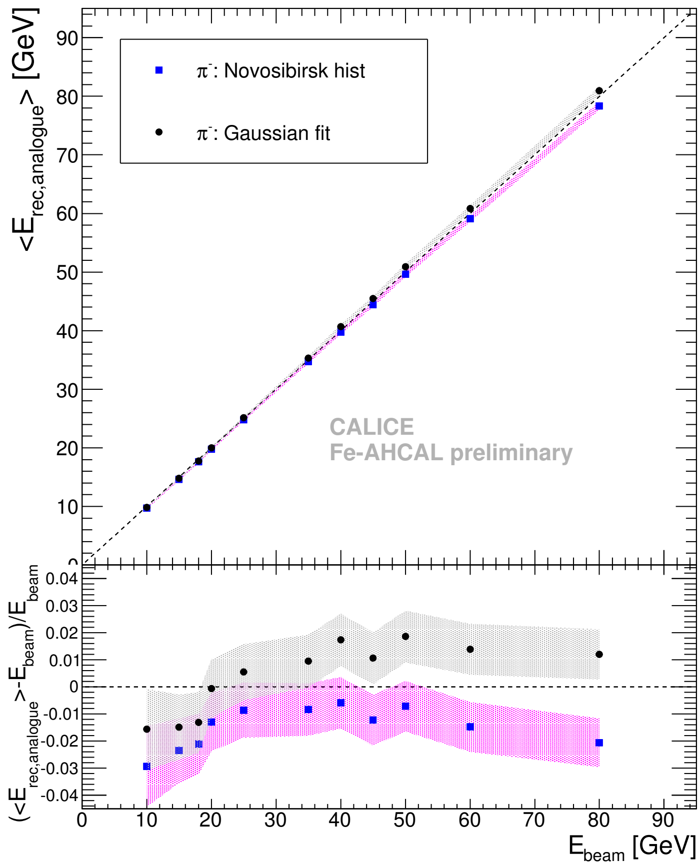

Figure 5: **Mean analogue reconstructed energy** for pion showers, the black dots show the most probable value taken from the Gaussian fit compared to the blue squares that show mean of the Novosibirsk filled distribution. The bands indicate statistical and systematic uncertainty added in quadrature, the statistical error only is smaller than the markers.

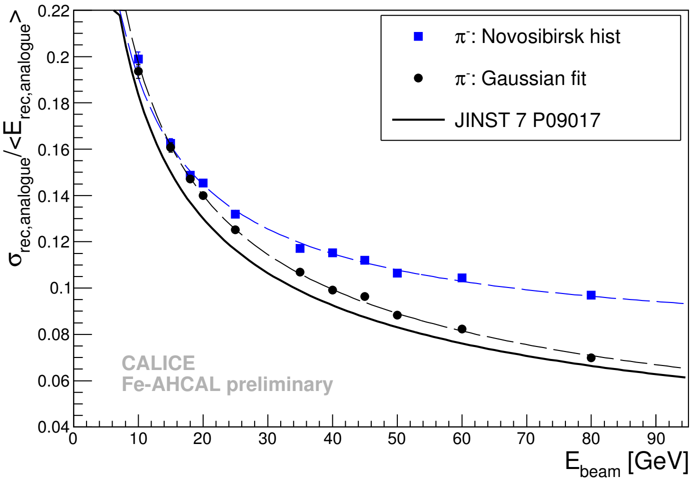

Figure 6: **Relative analogue energy resolution** as a function of the beam energy, shown in black dots for σ and $\langle E_{rec,analogue)}\rangle$ taken from the Gaussian fit, in blue squares the RMS and mean of the Novosibirsk filled distributions. For comparison the solid black line shows the AHCAL energy resolution with the whole test beam setup from [2].

that this effect is visible in this analysis because we neglect the TCMT contribution, contrary to the previous analysis. A slightly smaller effect was observed previously [11] when excluding the TCMT from the analysis of pion showers without a selection of the shower start.

The energy resolution as a function of the beam energy is fitted with equation 8. The results are summarised in table 2. The noise term c is fixed to the noise value for the ECAL and the AHCAL from [2]. Given the exclusion of the TCMT in the analyses, the “Gaussian fit” values are in reasonable agreement with the previous analysis [2]. For the “Novosibirsk hist” resolution, the degraded resolution at larger energies leads to a much larger constant term b in the fit.

Table 2: **Analogue energy resolution fit parameters** from equation 8. The uncertainties are only statistical.

	a [%]	b [%]	c [GeV]	χ^2/ndf
Gaussian fit	62.38 ± 0.45	1.24 ± 0.50	0.01	1.53
Novosibirsk hist	55.75 ± 0.59	7.36 ± 0.12	0.01	2.11
JINST 7 P09017	57.6 ± 0.4	1.6 ± 0.3	0.18	

4.1.2 Comparison between data and MC

The comparison of the analogue reconstructed energy distributions between data and simulation is shown in Figure 7. The response versus beam energy and the non-linearity is shown in Figure 8. Similar to the observations in the previous analysis [6], the FTFP_BERT predictions lie slightly below the data at low energies and exceed the data by a few percent at large energies.

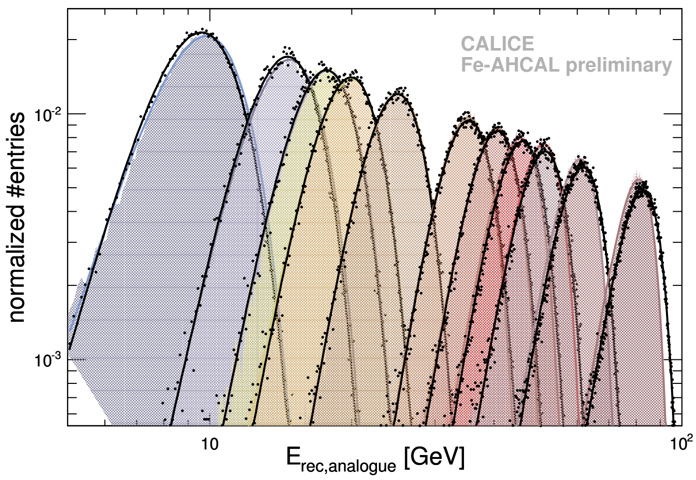

Figure 7: **Analogue reconstructed energy distributions** from 10-80 GeV for data and simulation. The filled and colored distributions show the data, the colored solid lines show the Novosibirsk fit to the data. The simulated FTFP_BERT distributions are shown with black dots, and the corresponding Novosibirsk fits with black solid lines.

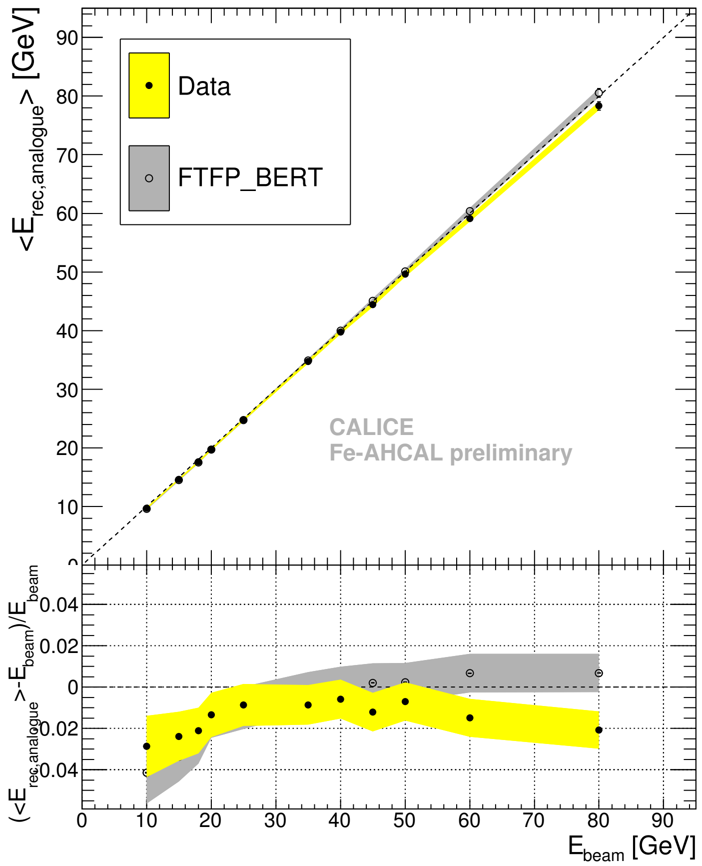

Figure 8: **Mean analogue reconstructed energy** for data in black dots and for simulated FTFP_BERT data in open black dots. All values determined by the same method. The bands indicate statistical and systematic uncertainty added in quadrature, the statistical error only is smaller than the markers.

4.2 Digital

The digital response is reconstructed from the number of hits above a threshold of 0.5 MIP, which is the value usually taken for AHCAL analyses ensuring a minimum noise level. This value isn't optimised. Examples for the distribution of the number of hits as well as the histograms filled from the Novosibirsk fit function are shown in Figure 9. The corresponding response, taken as the mean value of the filled Novosibirsk distribution, as a function of the beam energy is shown in Figure 10. The response is fitted with a power law $\langle N_{hits} \rangle = a \cdot (E_{beam})^b$ and the corresponding fit parameters are given in the caption. It shows a clear saturation behaviour. This is expected since the AHCAL granularity of (at best) 3x3 cm^2 cells is not well adapted to the digital reconstruction method, where several traversing particles contribute the same information to the reconstructed energy as a single traversing particle. In the bottom part of the Figure, the relative deviation of the reconstructed $\langle N_{hits} \rangle$ from the fit function is shown. For data and simulation, the point at 20 GeV deviates strongest from the fit curve. The non-linearity introduced by the saturation is corrected on an event-by-event basis by assuming $E_{rec,digital} = E_{beam}$ and inverting the fit functions, leading to

$$E_{rec,digital} = \sqrt[b]{\frac{N_{hits}}{a}}. \tag{9}$$

In the following, the parameters a and b extracted from the fit to the data are used to reconstruct the energy of the real and also for the simulated FTFP_BERT data.

The resulting $E_{rec,digital}$ distributions for data and simulation are compared in Figure 11. The histograms filled from the Novosibirsk fit function used to extract the the mean and the width of the $E_{rec,digital}$ distribution are also shown. After the correction of the saturation behaviour, the data show agreement with a linear behaviour within ±4 % (Figure 12). Since the simulation is corrected with the same function and parameters as the data, it shows slightly larger deviations from linearity than the data, with the largest deviation of $\sim 8\,\%$ at 20 GeV.

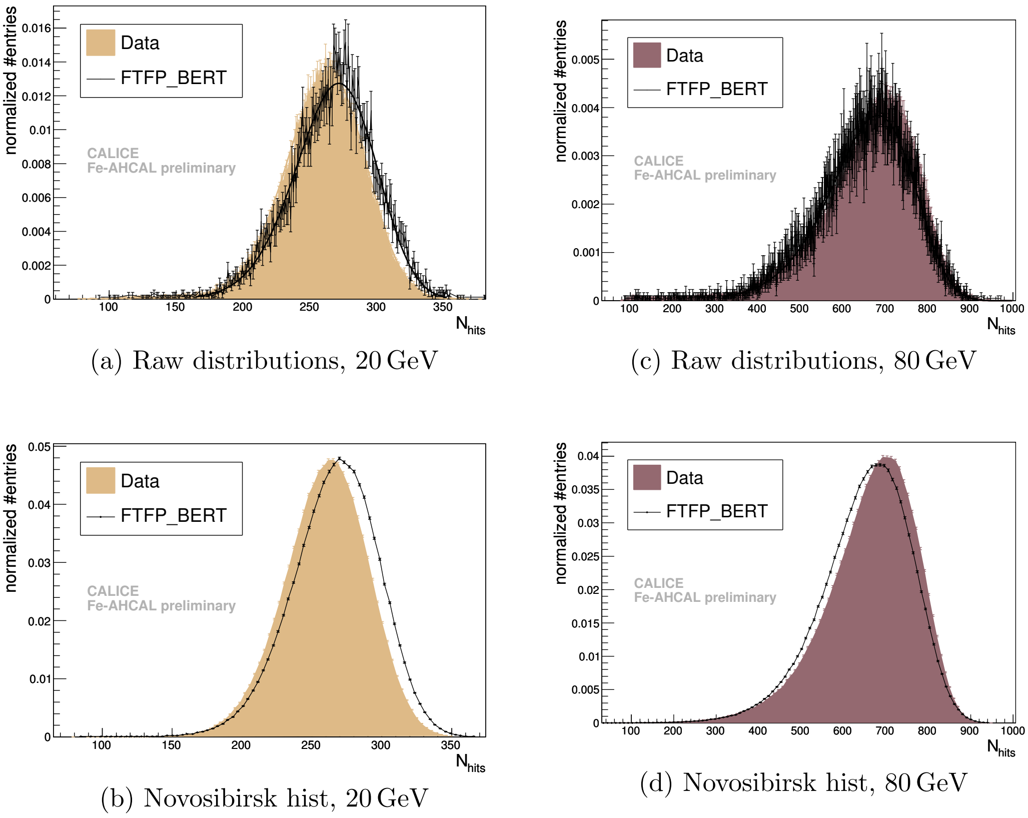

(a) Raw distributions, 20 GeV

(c) Raw distributions, 80 GeV

(b) Novosibirsk hist, 20 GeV

(d) Novosibirsk hist, 80 GeV

Figure 9: **Total number of hits distributions** for E_{beam} = 20 GeV and 80 GeV, data (colored) compared to simulation (black) distributions and the filled Novosibirsk distributions, from which the mean and the RMS are extracted.

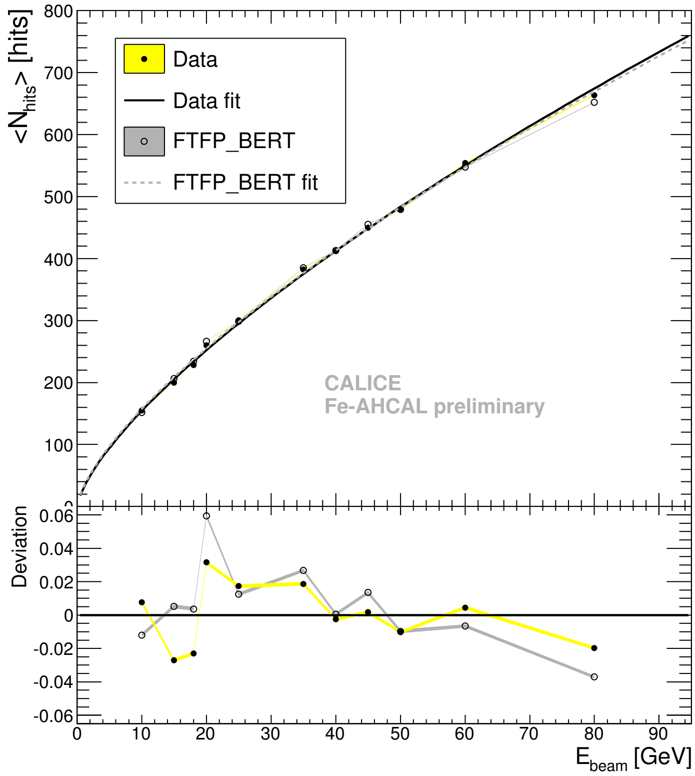

Figure 10: **Mean digital response** to pion showers, fitted with power law; data: $a = 30.06 \pm 0.06\,\mathrm{GeV}^{-b}$, $b = 0.710 \pm 0.001$, MC: $a = 31.60 \pm 0.06\,\mathrm{GeV}^{-b}$, $b = 0.697 \pm 0.001$. The plot on the bottom shows the deviation from power law fit. The bands indicate the statistical and systematic uncertainty added in quadrature, the statistical error only is smaller than the markers.

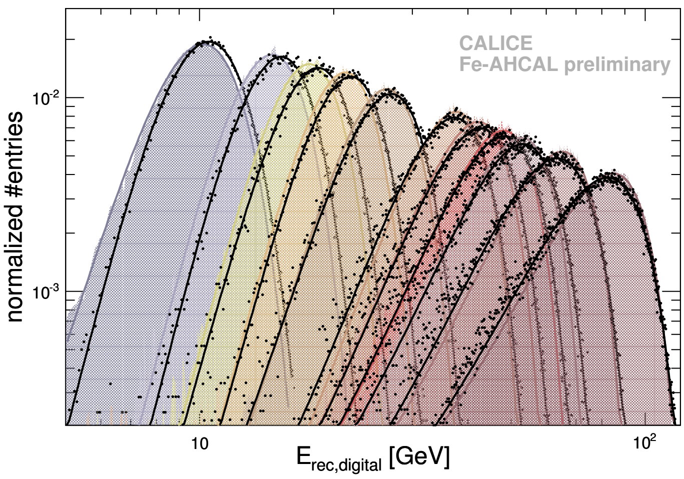

Figure 11: The **digital reconstructed energy distributions** are shown for all energies, data in colored filled histograms and FTFP_BERT simulated data in black dots. The black and colored curves show Novosibirsk fits.

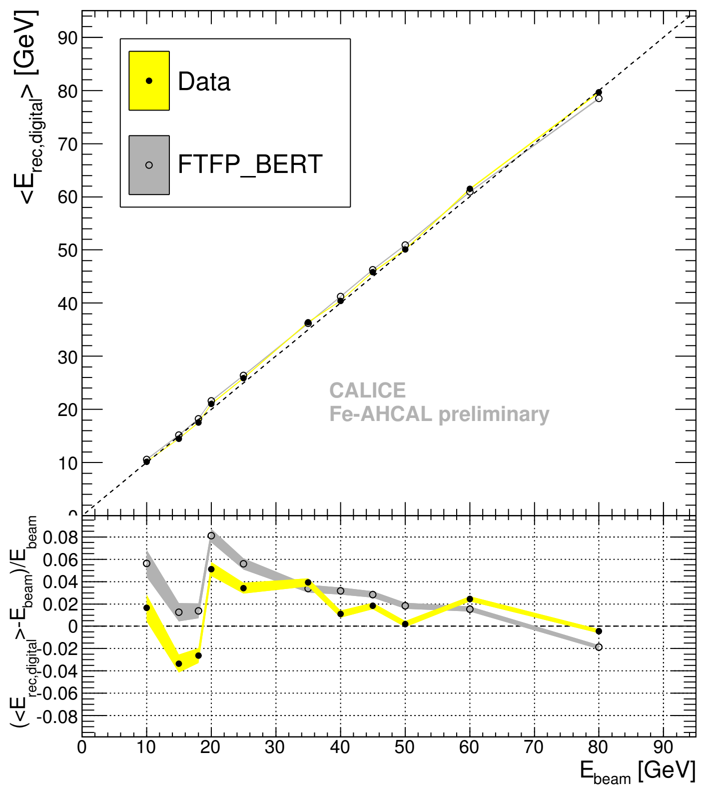

Figure 12: **Mean digital reconstructed energy** for pion showers, for data in black dots and for the FTFP_BERT simulation in open black dots. The bands indicate the statistical and systematic uncertainty added in quadrature, the statistical error only is smaller than the markers.

4.3 Semi-digital

The semi-digital energy reconstruction is done via equation 3, with N_1 = the number of hits below 5 MIP, N_2 =the number of hits above 5 MIP & below 15 MIP and N_3 =the number of hits above 15 MIP. These threshold values are adopted from the MICROMEGAS SDHCAL analysis [12]. They were not optimised for the AHCAL geometry which has a much larger cell size. The semi-digital response in terms of N_1,N_2 and N_3 is shown in Figure 13.

For the determination of the calibration coefficients α, β and γ the first 25.000 events of each energy data set are taken, and the χ^2-like function given in equation 4 is minimised. The resulting coefficients are shown in Figure 14.

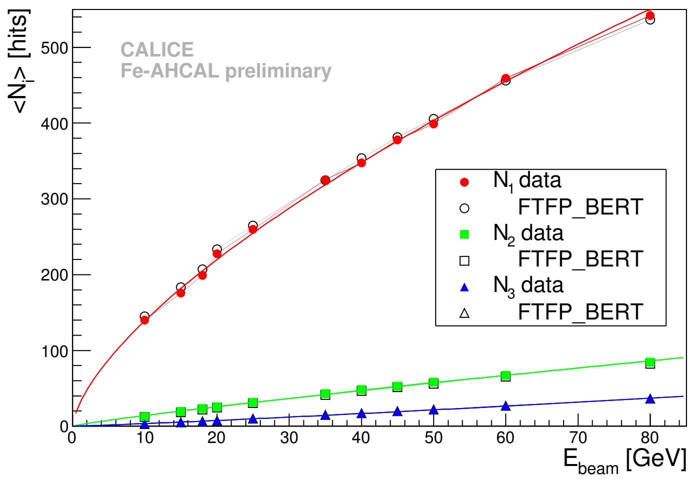

Figure 13: **Mean semi-digital response** to pion showers for data (filled colored markers) and MC (open markers); for hits above the first, below the second threshold N_1, hits above the second, below the third threshold N_2 and hits passing the third threshold N_3. The straight lines represent fits with a power law and the very small bands the statistical and systematic uncertainty added in quadrature.

Compared to the digital energy reconstruction, the semi-digital reconstruction leads to much smaller tails towards low energies. However, the non-linearity (Figure 15) looks stronger for data and simulation with deviations of +10 % at low energies and −5 % at large energies. This is an effect from the χ^2-like function, which implicitly assumes the uncertainty to scale with the square-root of the energy. An improved linearity can be reached by either using a different χ^2 definition, or by an additional

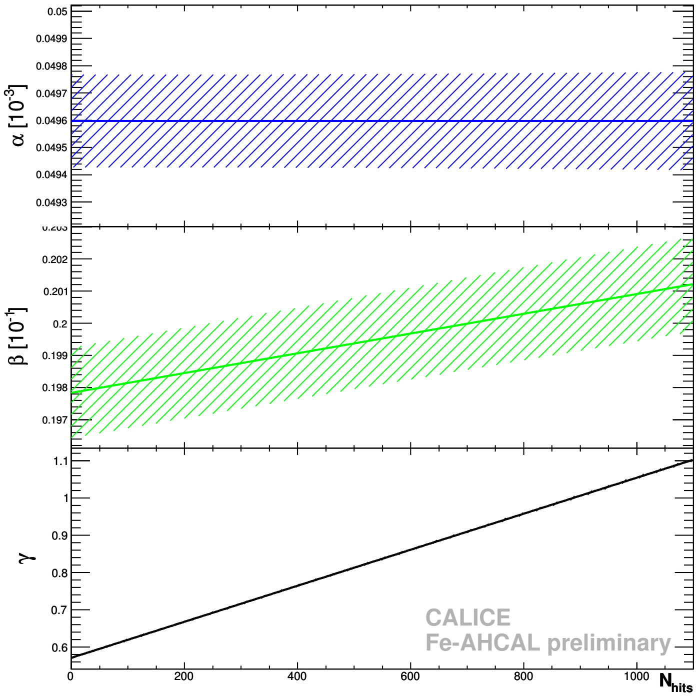

Figure 14: **Calibration coefficients** in the semi-digital energy reconstruction. The shaded area shows the statistical error.

linearisation step.

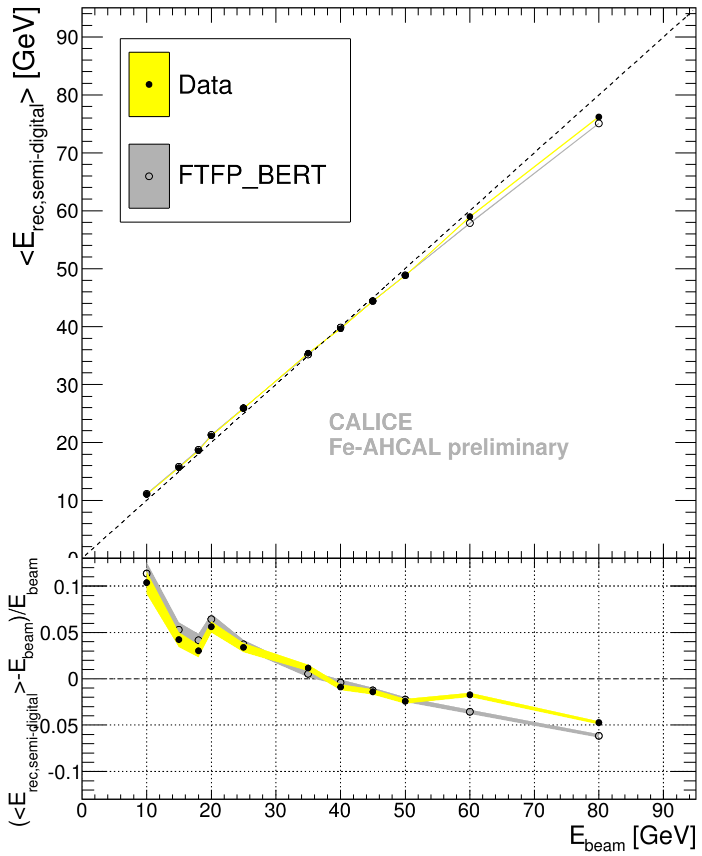

Figure 15: **Mean semi-digital reconstructed energy** for pion showers, for data in black dots and for simulated FTFP BERT data in open black dots. The bands indicate the statistical and systematic uncertainty added in quadrature, the statistical error only is smaller than the markers.

In order to compare with the other reconstruction methods, we apply a simple function to correct for this non-linearity. The resulting linearity is shown in Figure 16. In the following the semi-digital reconstructed energy is given as

$$E_{rec,SDcorr} = \sqrt[b]{\frac{E_{rec,semi-digital}}{a}} \tag{10}$$

with $a = 1.254 \pm 0.011\,\mathrm{GeV}^{-b}$ and $b = 0.9377 \pm 0.0022$ taken from the fit to data. In Figure 17 the distributions of the semi-digital reconstructed energy for data and simulated FTFP_BERT events are shown. A good agreement is observed for all

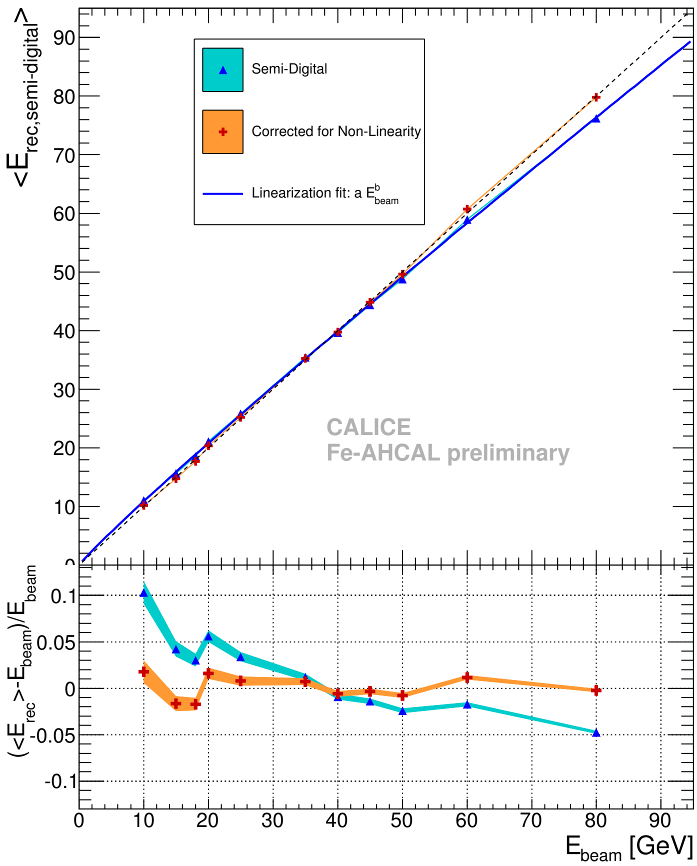

Figure 16: **Mean semi-digital reconstructed energy after linearity correction** for pion showers, for data before correction in blue triangles and after correction in red crosses. The bands indicate the statistical and systematic uncertainty added in quadrature, the statistical error only is smaller than the markers.

energies.

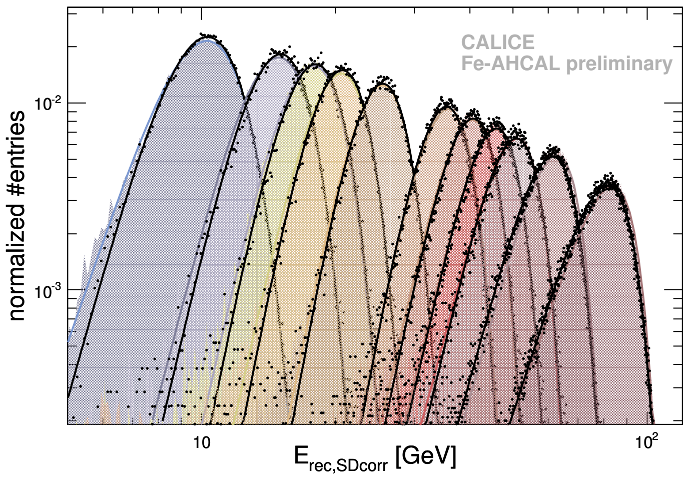

Figure 17: The **semi-digital reconstructed energy distributions** are shown for all energies, data in colored filled histograms and FTFP_BERT simulated data in black dots. The black and colored curves show Novosibirsk fits.

5 Energy resolution

Since all three reconstruction methods show a reasonable linearity, their resolutions can be compared. Since the AHCAL granularity is not optimised for the digital or semi-digital reconstruction method, large effects of the relatively large cell size on the resolution are expected at higher beam energies. The functional form usually employed to fit the relative energy resolution, equation 8, which consists of a stochastic, a constant and a noise term, does not accomodate for a larger resolution at higher energies. Therefore, we introduce a fourth term with variable exponent for the energy dependence, similar to the approach in [13]:

$$\frac{\sigma_{rec}}{\langle E_{rec} \rangle} = \frac{a}{\sqrt{E_{beam}[GeV]}} \oplus b \oplus \frac{c}{E_{beam}[GeV]} \oplus d \left(\frac{E_{beam}[GeV]}{100} \right)^e . \quad (11)$$

The fourth term can account for leakage as well as saturation effects. For each reconstruction method only those parameters are left free in the fit that are needed for a reasonable description of the data. A direct comparison of the extracted values between the different methods is therefore difficult, and the fits should mainly guide the eye.

5.1 Resolution of the analogue energy reconstruction

The relative resolution for the analogue energy reconstruction of the AHCAL pion data and of the corresponding FTFP_BERT simulation as a function of beam energy are shown in Figure 18. The simulation describes the data quite well for energies below 50 GeV. For higher energies the resolution of the simulated data lays about 0.5 % in absolute values above the data due to its 1 % better linearity (see Figure 8). Both show a decreasing relative resolution with increasing energy, as expected if leakage or saturation play only a minor role. Therefore, the resolutions can be parametrised with equation 8.

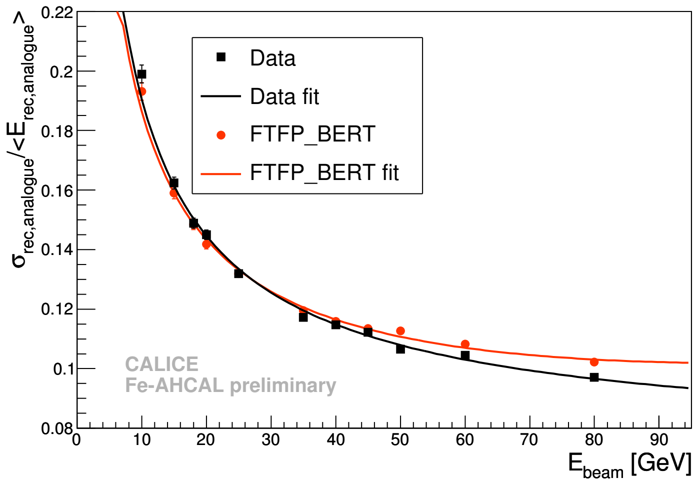

Figure 18: **Analogue energy resolution** for data and FTFP_BERT simulated events, both fitted with equation 11.

5.2 Resolution of the digital energy reconstruction

In Figure 19, the relative energy resolutions of the digital reconstruction method applied to AHCAL pion data and FTFP_BERT simulation are compared. Both data and simulation show a strong increase of the resolution towards large energies, and a minimum resolution of about 16 % for energies around 20 GeV, but the resolution curve in the simulation seems to be shifted to lower energies compared to the data. The strong rise at larger energies can be fitted when taking into account the fourth term in equation 11. Since the lowest beam energy used in this analysis is 10 GeV, the other terms decreasing with increasing energy in equation 11 are not well constrained. For this reason the values for a and b are fixed to zero in the fit to data and simulation.

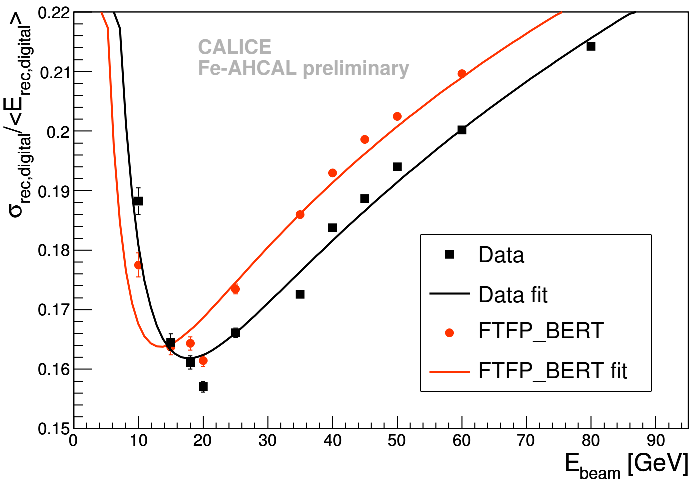

Figure 19: **Digital energy resolution** for data and FTFP_BERT simulated events, both fitted with equation 11.

5.3 Resolution of the semi-digital energy reconstruction

Also for the relative resolution of the semi-digital reconstruction method an increase at large energies is observed (Figure 20), but it is much less pronounced than for the digital reconstruction method. The resolution has a broad minimum in the energy range from about 25 GeV to 60 GeV with a minimum value of about 12 %. The simulation agrees well with the data in the whole analysed energy range. Similar to the fits to the digital energy resolution, the fourth term in equation 11 is needed for a good fit to data and simulation, and the first three terms more relevant and smaller energies are not well constrained. Here, the best fit is found when fixing b and c to zero.

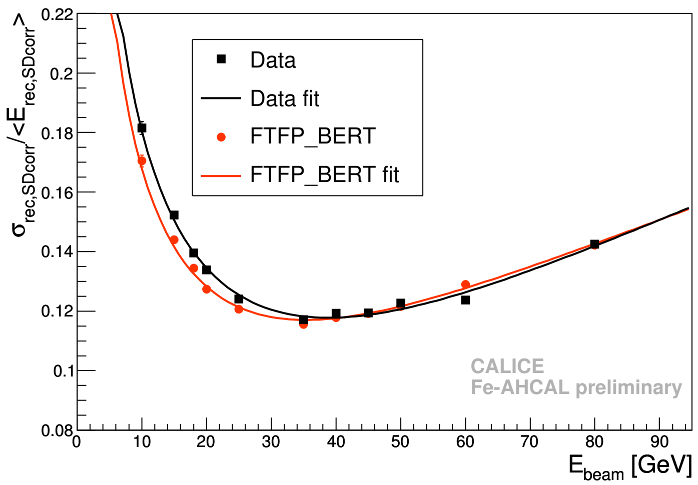

Figure 20: **Semi-digital energy resolution** for data and FTFP_BERT simulated events, both fitted with equation 11.

5.4 Comparison between different reconstruction procedures

The resolutions obtained with the different reconstruction methods applied to the same AHCAL data are compared directly in Figure 21. In addition, the best resolution reached with AHCAL data, by applying software compensation techniques [2], is indicated. For the comparison one should keep in mind that in the earlier analysis, the TCMT is fully included and the track in the ECAL considered in the energy reconstruction, while here a simplified treatment of the ECAL is used and the TCMT contribution is neglected.

The non-linearities of the three methods studied in this analysis are also shown in the lower part of Figure 21.

For the lowest energy points, the analogue and the digital reconstruction procedures show rather similar resolutions. For larger energies, the resolution of the analogue reconstruction method continues to decrease, while the digital resolution increases dramatically. The best resolution of all three methods for low energies up to about 35 GeV is found for the semi-digital reconstruction. It is however not better than the resolution reached with software compensation techniques. The semi-digital reconstruction and the software compensation both apply weights to the energy depositions in a shower which depend on hit energy or effectively shower density. At large energies, the analogue method shows the best resolution of the three reconstruction methods tested in this analysis.

The results obtained in this analysis are expected to depend on the cell size of the calorimeter and are therefore not directly applicable to the other calorimeter prototypes. For example, for the DHCAL and the SDHCAL prototypes the saturation is expected to become relevant only at considerably larger energies because of the smaller cell size. This is consistent with the fact that in the analysis of SDHCAL data, the resolutions obtained with a digital and the semi-digital reconstruction method agree up to energies of about 40 GeV, and the semi-digital procedure improves the resolution only for larger energies [5].

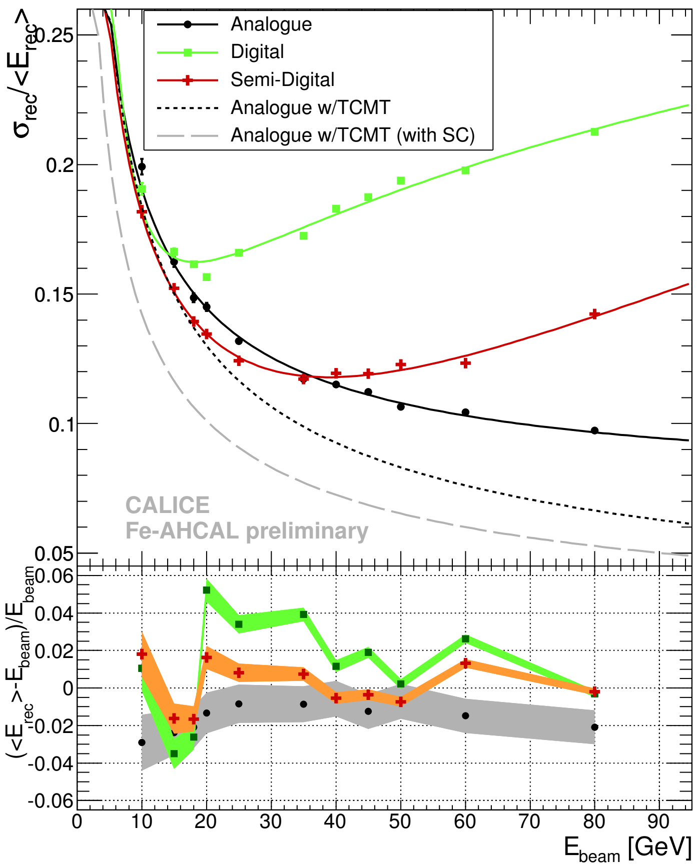

Figure 21: **Energy dependence of the relative energy resolution of the AHCAL** obtained using different approaches of the energy reconstruction for pions: analogue (black), digital (green) and semi-digital (red). The dashed and dotted curve show the resolution achieved in [2] with and without software compensation techniques, using the energy deposits in the TCMT (and of the track in the ECAL) in addition to the AHCAL. The bottom plot shows the residuals to beam energy with the bands indicating the systematic uncertainties and the statistical errors smaller than the markers.

6 Conclusions

Within the CALICE Collaboration, several techniques for highly granular hadronic calorimeters have been developed and tested in test beams of large prototypes. Different energy reconstruction methods are used for the different prototypes. The information measured by the analogue HCAL prototype can also be analysed with the reconstruction methods developed for the digital and the semi-digital HCAL, and thus allow a direct comparison of the three reconstruction methods by applying them to the same data sample. The methods are tested on pion test beam data collected in 2007 at CERN.

All three methods provide a reasonable linearity. The cell size of the AHCAL is not optimised for the digital and semi-digital reconstruction methods, leading to large saturation effects already below 30 GeV. The methods can correct for the shift of the mean number of hits due to the saturation, however the observed energy resolutions are significantly degraded. Of the three methods studied here, the semi-digital methods shows the best resolution below 30 GeV, while the resolution of the analogue reconstruction is best at large energies. None of the methods competes favourable with software compensation techniques using the full analogue information.

The results of this analysis are expected to depend significantly on the calorimeter cell size and thus are not directly applicable to the DHCAL or SDHCAL prototypes.

References

[1] CALICE Collaboration, Calibration of the Scintillator Hadron Calorimeter of ILD
CALICE Analysis Note CAN-018

[2] CALICE Collaboration, C. Adloff et al., Hadronic energy resolution of a highly granular scintillator-steel calorimeter using software compensation techniques
2012 JINST 7 P09017
doi:10.1088/1748-0221/7/09/P09017

[3] The CALICE collaboration et al., Electromagnetic response of a highly granular hadronic calorimeter
2011 JINST 6 P04003
doi:10.1088/1748-0221/6/04/P04003

[4] CALICE Collaboration, B. Bilki, The DHCAL Results from Fermilab test beams: CALibration
CALICE Analysis Note CAN-042

[5] CALICE Collaboration, G. Grenier, First results of the CALICE SDHCAL technological prototype
CALICE Analysis Note CAN-037

[6] CALICE Analysis Note CAN-040 , Pion and proton showers in the CALICE scintillator-steel AHCAL: comparison of global observables

[7] CALICE Collaboration et al., Validation of GEANT4 Monte Carlo models with a highly granular scintillator-steel hadron calorimeter
2013 JINST 8 P07005
doi:10.1088/1748-0221/8/07/P07005

[8] B. Lutz, Hadron Showers in a Highly Granular Calorimeter
DESY-THESIS-2010-048

[9] N. Feege, Low-energetic hadron interactions in a highly granular calorimeter,
DESY-THESIS-2011-048

[10] Djamel Boumediene (on behalf of the CALICE Collaboration) , Response of the CALICE Si-W ECAL Physics Prototype to electrons
2009 J. Phys.: Conf. Ser. 160 012065
doi:10.1088/1742-6596/160/1/012065

[11] CALICE Collaboration, C. Adloff et al., Construction and performance of a silicon photomultiplier/extruded scintillator tail-catcher and muon-tracker
2012 JINST 7 P04015
doi:10.1088/1748-0221/9/01/P01004

[12] CALICE Collaboration, M. Chefdeville, Off-line compensation of a SDHCAL, a Monte Carlo study
CALICE Collaboration Meeting in Hamburg,
20-22 March 2013

[13] M. A. Thomson, Particle Flow CALorimetry and the PandoraPFA Algorithm,
Nucl.Instrum.Meth.A611:25-40,2009
doi:10.1016/j.nima.2009.09.009

Appendix

A ECAL contribution to the energy reconstruction

Usually the ECAL contribution to the reconstructed energy is calculated by

$$E_{ECAL} = \sum_{k=1}^{3} \nu_k \cdot M_{ECAL,k} \tag{12}$$

with $M_{ECAL,k}$ is the energy sum in the ECAL layers with sampling fraction k. To approximate an reasonable offset, the E_{ECAL} was reconstructed with an average conversion factor, taken from [2], of $\sum_{k=1}^{3} \nu_k/3 = 0.005906$.
The resulting E_{ECAL} distribution for all selected pion events, thus with MIP like tracks in the ECAL, summed up over all energies is shown in Figure 22.
For an estimate the mean value is taken as the average energy deposited in the ECAL for the Analysis.

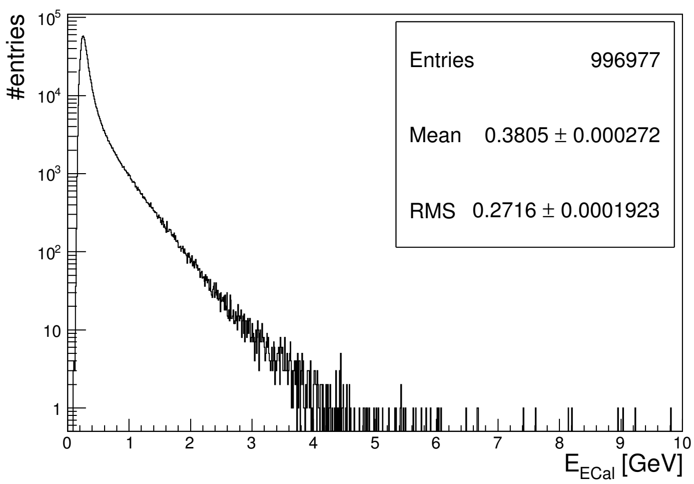

Figure 22: **Average reconstructed energy in the ECAL** for selected events with track in ECAL for all runs and energies.